Space vector pulse-width modulation technique for an eleven-phase voltage source inverter with sinusoidal output voltage generation

[1]Shaikh Moinoddin, [1]Haitham Abu-Rub, [2]Atif Iqbal, [1]SK Moin Ahmed, [3]Obrad Dordevic, [3]Emil Levi

[1]Electrical and Computer Engineering. Texas A&M University at Qatar, moinuddin2006@gmail.com, haitham.abu-rub@qatar.tamu.edu, moin.sk@qatar.tamu.edu
[2]Dept. of Electrical Engineering, Qatar University, Doha, Qatar, atif.iqbal@qu.edu.qa
[3]School of Engineering, Liverpool John Moores University, Liverpool, UK, e.levi@ljmu.ac.uk, o.dordevic@ljmu.ac.uk

Abstract: This paper discusses the space vector pulse width modulation (SVPWM) scheme for an eleven-phase two-level voltage source inverter (VSI), aimed at producing a sinusoidal output voltage waveform. Generalised space vector theory is used to realise the SVPWM. As per the general inverter switching theory, there are $2^{11} = 2048$ switching states that yield 2046 active voltage space vectors and one zero voltage vector, which results with two switching states. Out of the total of 2046 active voltage vectors, the most suitable set comprising 110 active voltage vectors is identified and is utilised in the implementation of the SVPWM. The sinusoidal voltage is obtained by controlling the duty cycles of the applied voltage space vectors in such a way that the non-zero reference voltage in the first (*d*-*q*) plane is achieved, while simultaneously zeroing the average voltage in the other four (*x*-*y*) planes in accordance with the zero references. The theoretical results are verified by experimentation using a passive resistive-inductive load. Finally, experimentally obtained THD values of the phase voltage and current for the eleven-phase SVPWM are compared with the corresponding values obtained using SVPWM for other odd phase numbers.

Keywords: Eleven-phase system, Multi-phase drives, Space vector PWM, Voltage source inverter.

I. INTRODUCTION

The area of multiphase drive systems has experienced a significant growth since the beginning of this century [1,2]. An increased interest in such drive realisations has been application-driven and aims at utilising various advantageous features that make multiphase machines an attractive solution for numerous applications associated with stringent fault tolerance requirements, high power industrial drives, remote offshore wind generation, and various means of electric transportation (e.g. locomotives, electric vehicles, electric ship, 'more electric' aircraft).

Variable-voltage, variable-frequency supply for multiphase (*m*-phase) drives is typically obtained using voltage source inverters, which can be either multilevel VSIs, that require multilevel multiphase PWM techniques [3-4], or two-level VSIs can be applied. This paper deals with a two-level VSI and hence further discussion relates to control of such a topology.

As the case is with all PWM techniques, regardless of the converter type, both three-phase and multiphase output voltage can be synthesised using either carrier-based or space vector PWM techniques [5]. Depending on the type of the machine used (with near-sinusoidal or with rectangular magneto-motive force distribution), the output voltage is required to contain either only the fundamental component or both the fundamental and a certain number of low-frequency higher odd harmonics [1,2]. Regardless of which of the two applies, realisation of the multiphase output with carrier-based PWM is simple and represents an extension of the well-known three-phase carrier-based PWM with zero-sequence (offset) injection. Sinusoidal output voltage synthesis is discussed in [6] while the multi-frequency output voltage generation principles are covered in [7]. While simple to implement, carrier-based PWM techniques do not enable a straightforward visualisation and analysis of the PWM process, which is one of the main reasons for resorting to space vector PWM techniques.

Following the pioneering work of [8], space vector PWM for two-level multiphase inverters has been explored in a considerable detail for various phase numbers. For example, five-phase VSI has been studied in [9,10], seven-phase VSI in [11] and nine-phase VSI in [12], all in conjunction with sinusoidal output voltage generation. Creation of a multi-frequency output voltage, based on the space vector approach, is described in [13,14] for the five-phase and seven-phase two-level VSIs.

Numerous PWM techniques, of both space vector and carrier-based type, have also been introduced for multiphase machines with an even phase number (e.g. asymmetrical and symmetrical six-phase machines [1,2]). However, such phase numbers do not conform to general rules, valid for odd phase numbers [8] and are therefore not discussed in details.

Reported survey shows that the space vector PWM technique for eleven-phase VSIs has not been introduced so far. Yet, eleven-phase variable speed drives are one of the potential solutions for various applications, that has been discussed extensively in recent times [15-17]. The purpose of this paper is therefore to develop a space vector PWM technique, which builds on the VSI modelling described in [18] and on the general space vector PWM principles exposed in [19], and which is aimed at sinusoidal output voltage generation. The VSI model is decomposed into five two-dimensional orthogonal spaces (planes). The switching combinations yield 2046 active space vectors, distributed across 22 sectors of 16.36° span, plus a zero vector with two switching states. Considering the constraints of the minimum number of semiconductor switchings and the sinusoidal output voltage waveform, only 110 active space vectors (plus two zero vector switching states) are needed. Ten active vectors and the zero vector

are chosen during each switching period to synthesise the sinusoidal reference voltage. Experimental results are provided to support the analytical and theoretical considerations.

Last but not least, a comparison of the total harmonic distortion (THD) of the phase voltage and current of the eleven-phase SVPWM, across the entire linear modulation region, with the corresponding THD values obtained using SVPWM in conjunction with other odd phase numbers is undertaken. The comparison is experimental and it includes three-, five-, seven- and nine-phase systems. It is shown that, if the switching frequency is kept constant, the lowest THD values for the phase voltage, and hence also for the load current under the condition of the passive load impedance, result with a three-phase system. This confirms the theoretical findings of [20].

II. Modelling of an 11-phase voltage source inverter

An eleven-phase VSI power circuit is shown in Fig. 1. All the considerations further on assume instantaneous commutation (no dead time) and zero forward voltage drop on semiconductor components. A constant dc input voltage is assumed and the output consists of phase-to-neutral voltages applied across the star-connected load, v_k, where k = 1, 2, 3, …, 11. The leg voltages are denoted as V_k. The output phase-to-neutral voltage v_k contains different levels. It can be expressed by using switching states (S_1, …, S_{11}, where S_k = 1 when the output of the leg k is connected to the positive rail, i.e. S_k = 0 when it is connected to the negative rail) as:

$$v_k = \left(S_k - \frac{1}{11} \sum S_k \right) \cdot V_{dc} \tag{1}$$

This equation shows how the phase voltage levels can be analytically determined from the switching states for a given dc-bus voltage. One can further conclude from (1) that the theoretical maximum difference in brackets results when S_k is equal to 1, and its sum with the other states is minimum, $\Sigma S_k = 1 + 10 \cdot 0$ (all other legs are 0). This gives the theoretical maximum phase voltage level in the eleven-phase case as equal to $v_k = 10/11 \cdot V_{dc}$. In a similar way one can conclude that the minimum voltage level is $v_k = -10/11 \cdot V_{dc}$. The step for the values of the phase voltages is defined with the minimum non-zero value of the sum in the brackets in (1):

$$v_{k\,\mathrm{step}} = \frac{1}{11} \cdot V_{dc}. \tag{2}$$

Hence the maximum possible number of levels achievable in the output phase-voltage of the eleven-phase two-level inverter is $2 \cdot (10/11 V_{dc}) / (1/11 V_{dc}) + 1 = 21$ (10 positive levels, 10 negative and zero). This will be confirmed further on through the experimental results.

An eleven-phase system can be described with an 11-dimensional vector in the 11-dimensional space. Such a multidimensional vector can be conveniently represented, using the concept of multiple orthogonal planes, with two-dimensional (2D) space vectors in five planes, plus a zero-sequence component. The space vectors in the 2D planes, denoted further on as the d-q plane (flux and torque production due to the fundamental component), and x-y planes (x_1-y_1, x_2-y_2, x_3-y_3, x_4-y_4 planes, with zero reference voltage vectors) are defined using power variant transformation [1,2] as follows:

$$\overline{V}_{\mathrm{plane}} = \frac{2}{11} \sum_{k=1}^{11} V_k e^{j \frac{2\pi}{11}(k-1)\,pl} \tag{3}$$

where k is the phase number in accordance with notation in Fig. 1, index 'plane' stands for the relevant plane (d-q, x_1-y_1, …, x_4-y_4) and variable pl takes the values pl = 1 for the d-q plane, pl = 2 for the x_1-y_1 plane, and so on, up to pl = 5 for the x_4-y_4 plane. The zero-

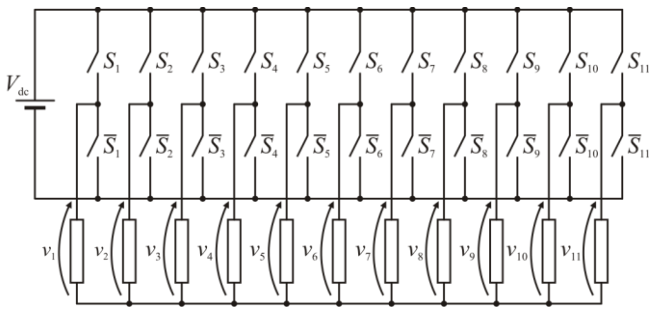

Fig. 1. 11-phase voltage source inverter's power circuit.

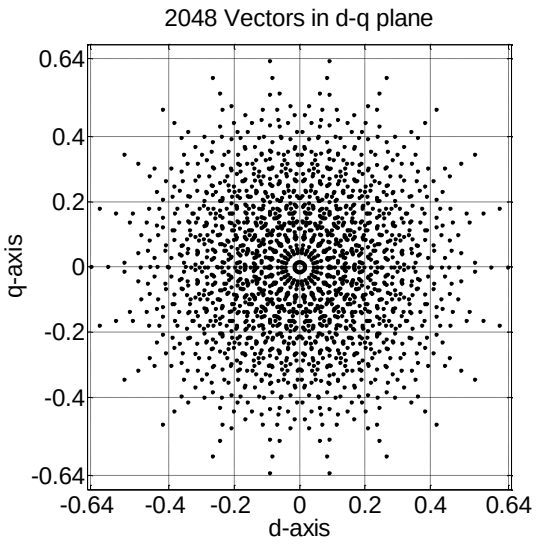

Fig. 2. All the possible phase voltage space vectors (2046 active plus zero with two switching states) for an 11-phase inverter. Values are given in per unit, normalised with respect to the dc voltage (the same applies to subsequent figures).

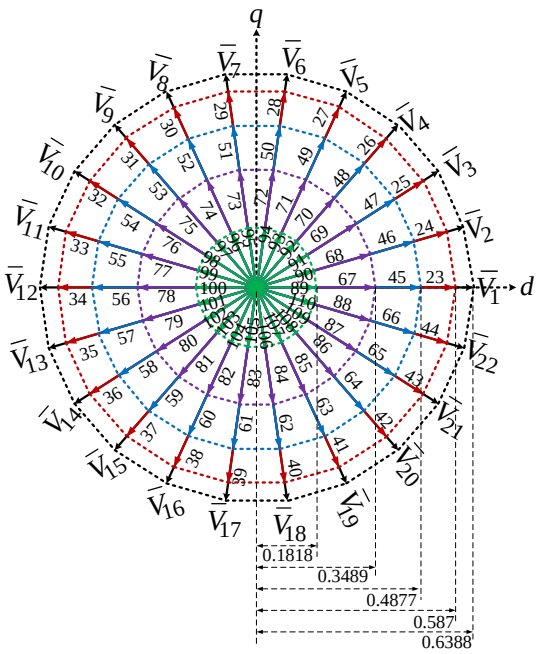

Fig. 3. Voltage space vectors selected for SVPWM implementation (110 active vectors) in the d-q plane for an 11-phase VSI. Sector-I is from 0º to 16.36º, sector-II from 16.36º to 32.72º, and so on.

sequence component, which will map into the common mode voltage due to the assumed isolated neutral of the star connection of the load, is governed with:

$$V_0 = \frac{1}{11}\sum_{k=1}^{11} V_k \tag{4}$$

The complete space vector set in the *d-q* plane can be plotted, using (3) for *pl* = 1, as shown in Fig. 2. The disposition of the space vectors in all four *x-y* planes is the same, but different vectors appear at different positions and have different magnitudes. Thus the number of different space vector projections is the same in all planes (in contrast to, for example, a nine-phase system; this is so since eleven is a prime number). The condition that the total number of switchings is the minimum possible is imposed as the requirement for the space vector modulation. The switching pattern also has to be symmetrical, as the case is in standard three-phase SVPWM [5]. This translates into a single switching of each semiconductor in each switching half-period and severely restricts the number of active vectors that are to be used. Next, if a particular switching configuration (e.g. five upper and six lower switches on) offers a multitude of space vector sets with different magnitudes, the selected space vector sets are always those of the highest magnitude [8]. Last but not least, SVPWM that will provide full control over all five planes has to utilise ten active vectors plus the zero vector (with both switching states) in each switching period. These are, in essence, the same prerequisites that have been already used in the development of the SVPWM for e.g. five-phase [9,10], seven-phase [11] and nine-phase [12] VSIs.

These constraints lead to the selection of 110 active space vectors for further consideration, which are illustrated in Fig. 3. Five sets of 22 active vectors with different magnitudes are chosen (the magnitudes are given in per-unit, and are normalized with respect to V_{dc}). The mapping of the selected 110 active vectors in the additional *x-y* planes is shown in Fig. 4, which demonstrates that the length and position of a particular space vector is different in different planes. The space vectors are numbered in sequence starting from 1 to 22 in the outermost polygon of the *d-q* plane, Fig. 3, followed by 23-44, 45-66, 67-88 and 89-110 in the subsequent polygons of reducing vector magnitudes. The same numbering is preserved in the other planes, so that the mapping of the vectors in the four *x-y* planes can be easily followed. The mapping is summarised in Table 1.

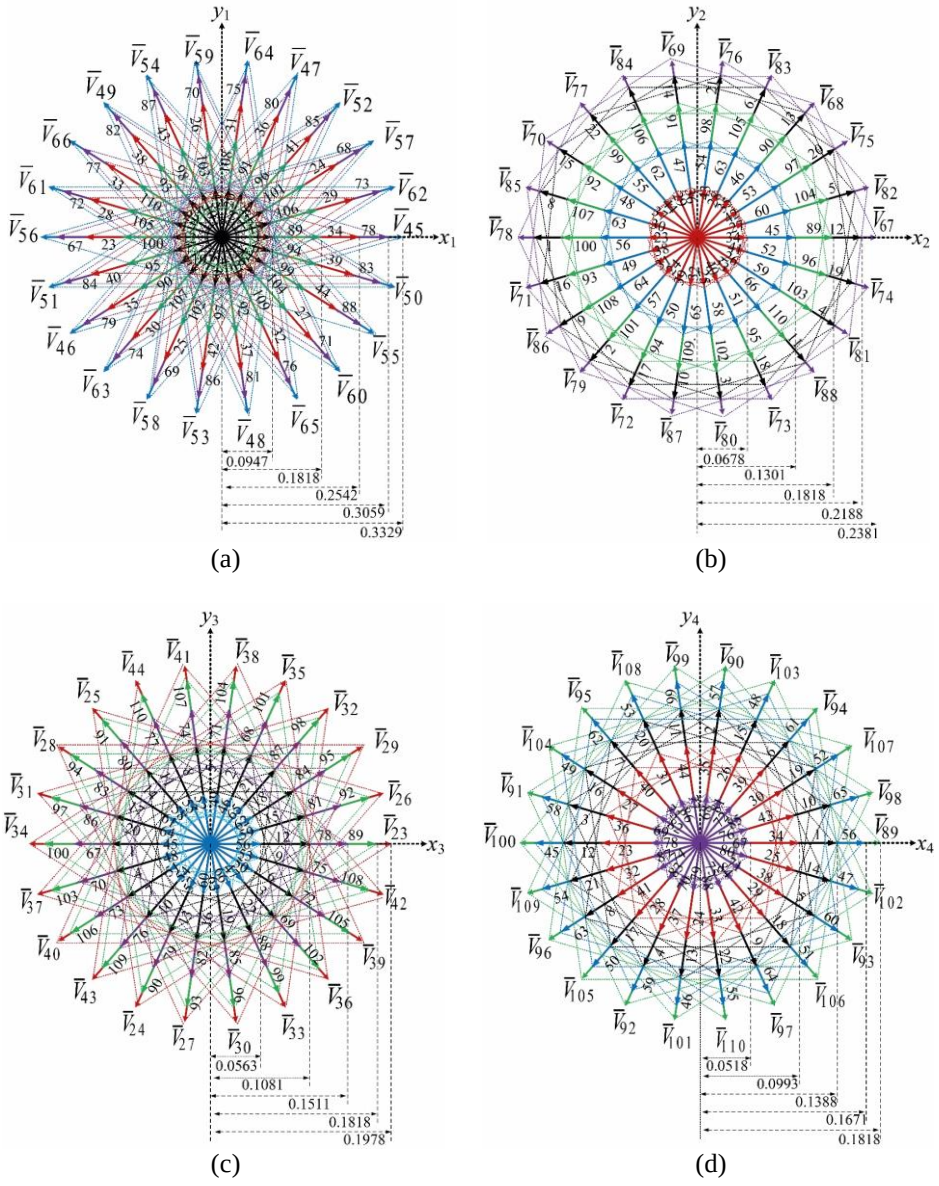

Fig. 4. Mapping of the active voltage space vectors, selected for SVPWM to realise the reference in the *d-q* plane (110 in total), in (a) x_1-y_1 plane; (b) x_2-y_2 plane; (c) x_3-y_3 plane; (d) x_4-y_4 plane.

Table 1. Mapping of the voltage space vectors of an 11-phase VSI.

Vector number		*d-q* plane	x_1-y_1 plane	x_2-y_2 plane	x_3-y_3 plane	x_4-y_4 plane	Vector colour in figure
1-to-22	Polygon no.*	1	5	2	4	3	Black
	Magnitude	0.6388	0.0947	0.2188	0.1081	0.1388	
23-to-44	Polygon no.	2	3	5	1	4	Red
	Magnitude	0.5870	0.2542	0.0678	0.1978	0.0993	
45-to-66	Polygon no.	3	1	4	5	2	Blue
	Magnitude	0.4877	0.3329	0.1301	0.0563	0.1671	
67-to-88	Polygon no.	4	2	1	3	5	Purple
	Magnitude	0.3489	0.3059	0.2381	0.1511	0.0518	
89-to-110	Polygon no.	5	4	3	2	1	Green
	Magnitude	0.1818	0.1818	0.1818	0.1818	0.1818	

*Outermost polygon is no. 1 and the innermost one is no. 5.

III. SPACE VECTOR PWM SYNTHESIS

As can be seen in Fig. 3, there are 22 sectors that each span 16.36°. The following discussion is limited to one odd (sector-I) and one even (sector-II) sector and the same concept applies to all the other odd and even sectors. As per the general rule of space vector PWM [8], 10 active space vectors are needed to yield sinusoidal output, along with two switching states of the zero space vector. In sector-I, active vectors 89, 68, 45, 24, 1, 2, 23, 46, 67, 90 are used in the listed order in the first half of the switching period; in the second half the same vectors are used in the reverse order, to yield symmetrical PWM. The active space vectors used in sector-II are 91, 68, 47, 24, 3, 2, 25, 46, 69, 90 in the first half of the switching period followed by their mirror image in the second half of the switching period. The disposition of applied voltage space vectors is shown in Fig. 5 for the sector-I and sector-II.

The switching pattern in Fig. 5 shows that the switches change their states at different instants of time. The total number of switching actions in each switching period is 22 (two switchings per leg), thus ensuring that the requirement that each switch is turned once 'on' and once 'off' in the switching period is met.

The selected space vectors in sector-I are shown in Fig. 6a in the *d-q* plane, and their mapping into the other (*x-y*) planes is depicted in Figs. 6b-6e. As can be seen from Figs. 6b-6e, the selected vectors are in all four *x-y* planes positioned along two straight lines, and there are vectors in phase opposition. By an appropriate adjustment of the application times of the vectors, it is possible to cancel vectors in phase opposition and thus achieve on average zero reference values in all four *x-y* planes. In this way, only the non-zero reference in the *d-q* plane is realised and the output voltage waveform will be completely sinusoidal, except for the switching harmonics. If the inverter were to be operated in the 180° conduction mode, 22-step operation would result, yielding the maximum peak of the fundamental output equal to [18]

$$V_{\max,22-\text{step}} = \frac{2}{\pi} V_{dc} = 0.6366 V_{dc} \tag{5}$$

In an alternative space vector PWM, which follows the analogy with the three-phase SVPWM and uses only two active vectors per sector (and is therefore unable to provide zero average voltages in the *x-y* planes), the maximum fundamental peak output voltage $V_{\max}$ can be obtained by determining the radius of the largest inscribed circle,

$$V_{\max} = \frac{2V_{dc}}{11} \frac{\sin\left(\frac{5\pi}{11}\right)\cos\left(\frac{\pi}{22}\right)}{\sin\left(\frac{\pi}{11}\right)} = 0.6323 V_{dc} \tag{6}$$

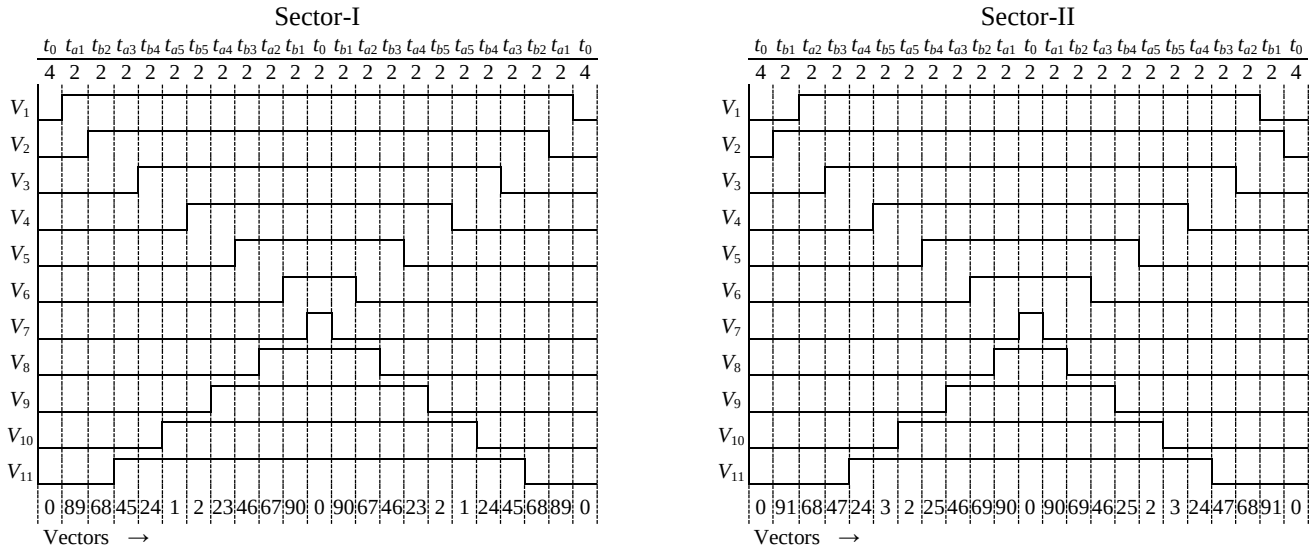

(a) (b)

Fig. 5. (a) Switching pattern and space vector disposition for one switching period, showing use of 10 active vectors along with two switching states of the zero vector in: (a) sector-I (vectors 1, 2, 23, 24, 45, 46, 67, 68, 89, 90); (b) sector-II (vectors 2, 3, 24, 25, 46, 47, 68, 69, 90, 91).

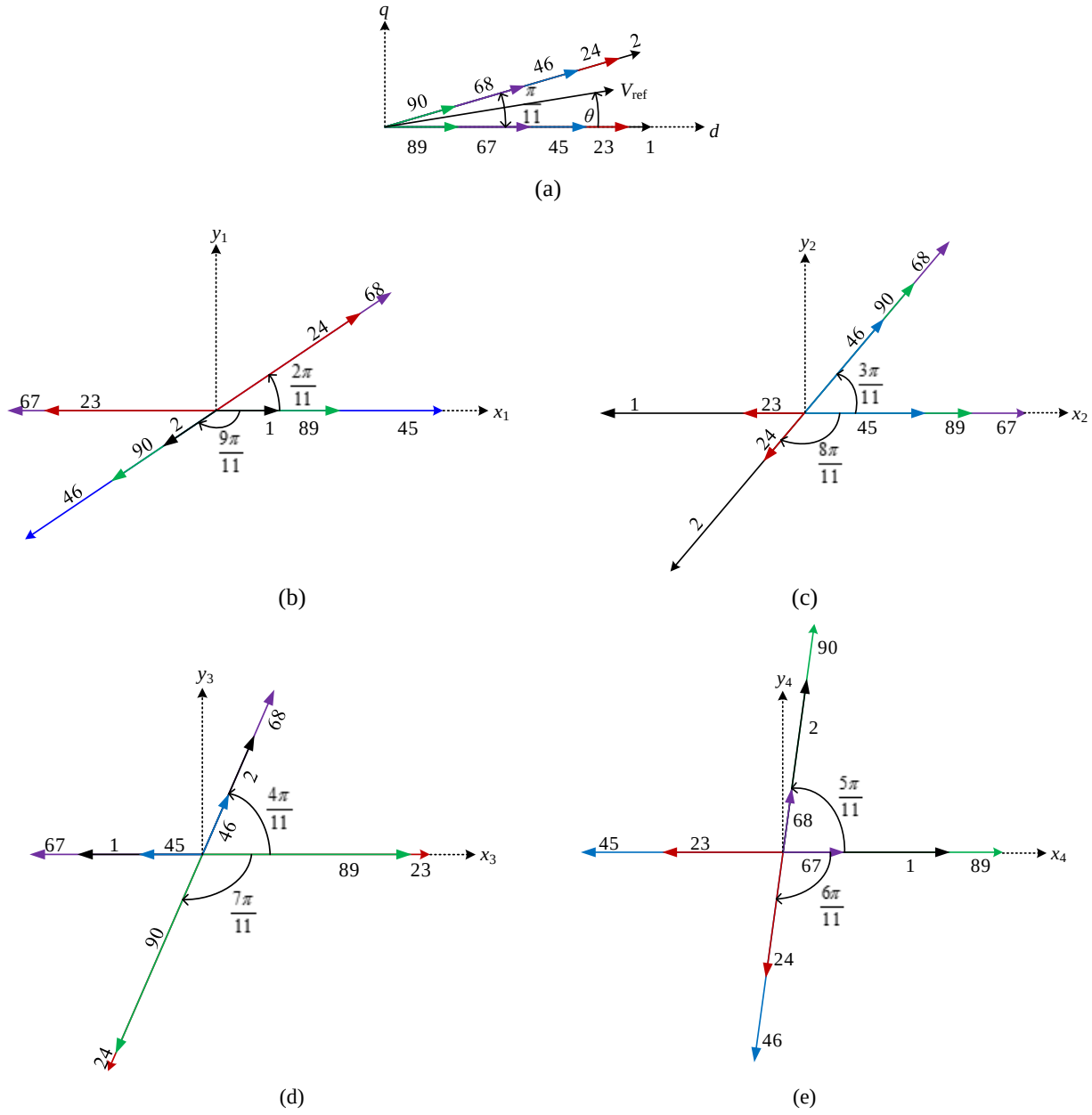

Fig. 6. Projections of selected active space vectors for sector-I in: (a) *d*-*q* plane; (b) x_1-y_1 plane; (c) x_2-y_2 plane; (d) x_3-y_3 plane; (e) x_4-y_4 plane.

In the full PWM operation that enables zeroing on average of the voltages in all the *x*-*y* planes and therefore uses 10 active vectors, the maximum achievable peak fundamental output voltage is considerably lower than the values given with (5)-(6). It is governed with:

$$V_{\max-\mathrm{PWM}} = M_{\max} V_{dc} / 2 = 0.50514 V_{dc} \tag{7}$$

where M stands for the modulation index, defined as $M = V_{\mathrm{ref}}/(0.5V_{dc})$ and its maximum value is $M_{\max} = 1.0103$, since $M_{\max} = 1/\cos(\pi/(2m))$ [6]. Hence the price paid for zeroing the average voltages in all *x*-*y* planes is the maximum modulation index $M_{\max}$ in the linear modulation region that is insignificantly higher than one.

In what follows the calculation of the application times of the applied vectors is discussed. For this purpose it is convenient to introduce the following constant [19]:

$$K_p = \sin(p\frac{\pi}{11}) \tag{8}$$

where p = 1, 2, 3, 4, 5. Let the duty cycle of any applied space vector be given with a general expression $\delta = t/t_s$, where t_s is the switching period. A solution for duty cycles of the active space vectors used for the 11-phase SVPWM for sinusoidal output voltage generation can be written as [19]:

$$\begin{bmatrix}\delta_{a1}\\ \delta_{a2}\\ \vdots\\ \delta_{a5}\end{bmatrix} = \begin{bmatrix}K_1\\ K_2\\ \vdots\\ K_5\end{bmatrix} M\sin(s\frac{\pi}{11}-\theta)$$
$$\begin{bmatrix}\delta_{b1}\\ \delta_{b2}\\ \vdots\\ \delta_{b5}\end{bmatrix} = \begin{bmatrix}K_1\\ K_2\\ \vdots\\ K_5\end{bmatrix} M\sin(\theta-(s-1)\frac{\pi}{11}) \tag{9}$$

where s stands for the sector number (s = 1…22), θ is the angular position of the reference voltage space vector in the first plane (as shown in Fig. 6a), and a and b relate to the active vectors along sector dividing lines, used in any particular sector. Indices 1-5 stand for the used vectors ordered from the smallest to the largest

(e.g., in sector-I the vectors *a*1 to *a*5 are vectors 89, 67, 45, 23, 1, while vectors *b*1 to *b*5 are vectors 90, 68, 46, 24, 2). Duty cycle of the zero space vector (which will be subdivided into two equal parts for the two switching states) is:

$$\delta_0 = [1 - K_5 M \cos((2s-1)\frac{\pi}{22} - \theta)] \tag{10}$$

Once when duty cycles have been calculated, they need to be summed properly in order to obtain per-leg duty cycles that will be distributed in accordance with the current sector. This requires knowledge of the sequence of space vectors within the switching period. As shown in Fig. 5, symmetrical switching pattern is assumed, which means that one state of the zero space vector appears at the beginning and at the end of the switching period, while the other state appears in the middle of the switching period. The sequence in sector-I starts with the smallest *a*1 space vector and changes in an alternating manner, through the selected set of active space vectors, ending with the smallest *b*1 space vector. The sequence is then reversed during the second half of the switching period and is a mirror image of the sequence from the first half of the switching period. Although illustrations in Fig. 5 are for the first and the second sector, the same applies to all the other odd (even, respectively) sectors.

Based on these considerations, it is possible to arrive at the set of expressions that yield the values of the final per-leg duty cycles. In all odd sectors (superscript *O*) of an 11-phase SVPWM, per-leg duty cycles (11 of them), in increasing order, can be calculated as:

$$\delta_1 = \frac{\delta_0}{2}$$

$$\begin{bmatrix} \delta_2^O \\ \delta_3^O \\ \delta_4^O \\ \vdots \\ \delta_6^O \\ \delta_7^O \\ \vdots \\ \delta_9^O \\ \delta_{10}^O \\ \delta_{11} \end{bmatrix} = \begin{bmatrix} 0 & 0 & 0 & \cdots & 0 & 0 & \cdots & 0 & 0 & 1 \\ 0 & 0 & 0 & \cdots & 0 & 0 & \cdots & 0 & 1 & 1 \\ 0 & 0 & 0 & \cdots & 0 & 0 & \cdots & 1 & 1 & 1 \\ \cdots & \cdots & \cdots & \cdots & \cdots & \cdots & \cdots & \cdots & \cdots & \cdots \\ 0 & 0 & 0 & \cdots & 0 & 1 & \cdots & 1 & 1 & 1 \\ 0 & 0 & 0 & \cdots & 1 & 1 & \cdots & 1 & 1 & 1 \\ \cdots & \cdots & \cdots & \cdots & \cdots & \cdots & \cdots & \cdots & \cdots & \cdots \\ 0 & 0 & 1 & \cdots & 1 & 1 & \cdots & 1 & 1 & 1 \\ 0 & 1 & 1 & \cdots & 1 & 1 & \cdots & 1 & 1 & 1 \\ 1 & 1 & 1 & \cdots & 1 & 1 & \cdots & 1 & 1 & 1 \end{bmatrix} \cdot \begin{bmatrix} \delta_{b1} \\ \delta_{a2} \\ \delta_{b3} \\ \vdots \\ \delta_{b5} \\ \delta_{a5} \\ \vdots \\ \delta_{a3} \\ \delta_{b2} \\ \delta_{a1} \end{bmatrix} + \delta_1 \tag{11}$$

For even sectors (superscript *E*), basically the same calculations can be applied, but this time with the reversed sequences of the duty cycles of active space vectors, in accordance with the reversed sequence of active space vectors. Therefore:

$$\delta_1 = \frac{\delta_0}{2}$$

$$\begin{bmatrix} \delta_2^E \\ \delta_3^E \\ \delta_4^E \\ \vdots \\ \delta_6^E \\ \delta_7^E \\ \vdots \\ \delta_9^E \\ \delta_{10}^E \\ \delta_{11} \end{bmatrix} = \begin{bmatrix} 0 & 0 & 0 & \cdots & 0 & 0 & \cdots & 0 & 0 & 1 \\ 0 & 0 & 0 & \cdots & 0 & 0 & \cdots & 0 & 1 & 1 \\ 0 & 0 & 0 & \cdots & 0 & 0 & \cdots & 1 & 1 & 1 \\ \cdots & \cdots & \cdots & \cdots & \cdots & \cdots & \cdots & \cdots & \cdots & \cdots \\ 0 & 0 & 0 & \cdots & 0 & 1 & \cdots & 1 & 1 & 1 \\ 0 & 0 & 0 & \cdots & 1 & 1 & \cdots & 1 & 1 & 1 \\ \cdots & \cdots & \cdots & \cdots & \cdots & \cdots & \cdots & \cdots & \cdots & \cdots \\ 0 & 0 & 1 & \cdots & 1 & 1 & \cdots & 1 & 1 & 1 \\ 0 & 1 & 1 & \cdots & 1 & 1 & \cdots & 1 & 1 & 1 \\ 1 & 1 & 1 & \cdots & 1 & 1 & \cdots & 1 & 1 & 1 \end{bmatrix} \cdot \begin{bmatrix} \delta_{a1} \\ \delta_{b2} \\ \delta_{a3} \\ \vdots \\ \delta_{a5} \\ \delta_{b5} \\ \vdots \\ \delta_{b3} \\ \delta_{a2} \\ \delta_{b1} \end{bmatrix} + \delta_1 \tag{12}$$

Table 2. Per-leg duty cycle disposition through sectors.

Leg\Sector	**1**	**2**	**3**	**…**	**11**	**12**	**…**	**20**	**21**	**22**
1	δ_{11}	δ_{10}^E	δ_9^O	**…**	δ_1	δ_1	**…**	δ_9^E	δ_{10}^O	δ_{11}
2	δ_{10}^O	δ_{11}	δ_{11}	**…**	δ_3^O	δ_2^E	**…**	δ_7^E	δ_8^O	δ_9^E
3	δ_8^O	δ_9^E	δ_{10}^O	**…**	δ_5^O	δ_4^E	**…**	δ_5^E	δ_6^O	δ_7^E
⋮	⋮	⋮	⋮	**…**	⋮	⋮	**…**	⋮	⋮	⋮
6	δ_2^O	δ_3^E	δ_4^O	**…**	δ_{11}	δ_{10}^E	**…**	δ_2^E	δ_1	δ_1
⋮	⋮	⋮	⋮	**…**	⋮	⋮	**…**	⋮	⋮	⋮
9	δ_5^O	δ_4^E	δ_3^O	**…**	δ_6^O	δ_7^E	**…**	δ_8^E	δ_7^O	δ_6^E
10	δ_7^O	δ_6^E	δ_5^O	**…**	δ_4^O	δ_5^E	**…**	δ_{10}^E	δ_9^O	δ_8^E
11	δ_9^O	δ_8^E	δ_7^O	**…**	δ_2^O	δ_3^E	**…**	δ_{11}	δ_{11}	δ_{10}^E

It can be seen from (11) and (12) that the smallest per-leg duty cycle (δ_1) corresponds to the application of the zero space vector in the middle of the switching period, while the largest duty cycle (δ_{11}) is the result of summation of δ_1 and all the active space vector duty cycles.

Finally, once when per-leg duty cycles are calculated, they need to be distributed properly among inverter legs depending on the current sector. It is enough to consider situation with respect to the first inverter leg 1. It can be observed that in the first 11 sectors duty cycles are, for the first inverter leg, in the order from the largest one to the smallest one, respecting the odd/even sector relations. Then, in the remaining 11 sectors, the order of duty cycles is reversed, and they are applied from the smallest one to the largest one, again respecting the odd/even sector relations (Table 2, row 1). For all the other inverter legs, duty cycle disposition is obtained by simple shifting of the sequence of the previous leg by two sectors. Since sectors span $\pi/11$, this is effectively a shifting of $2\pi/11$ radians. Thus, disposition for leg 2 is obtained by shifting duty cycles of leg 1 by two sectors, leg 3 receives resulting duty cycles of leg 2 shifted again by two sectors, and so on. In this way, duty cycle disposition for all 11 inverter legs in all 22 sectors is obtained. This is summarised in Table 2.

Although the SVPWM is selected for practical implementation in this paper, it should be noted that, when the desired output is a sinusoidal waveform, there is not much difference between space vector and carrier-based PWM modulation techniques. To be more precise, both modulation strategies can yield the same performance by proper adjustment of the sub-division of the time of the redundant switching states (that is, the zero vector) in SVPWM, i.e. by adjusting an appropriate offset in the carrier-based PWM. For example, if the times of application are equally shared in the SVPWM algorithm (as the case is in this paper), the same performance can be obtained by using carrier-based PWM with min-max injection. This applies to any number of phases. However, the benefit of using SVPWM is, as always, that it gives better insight into the modulation process, as it was demonstrated in this paper for the eleven-phase case.

IV. Experimental results

Based on the theory presented in the previous section, space vector algorithm has been implemented in the laboratory. For the experimental verification, dSpace ds1006 has been used for real-time implementation of the described algorithm. Two two-level custom-made inverters (each with up to 8 outputs), were connected in parallel to the same dc link in order to create an 11-phase system. Semiconductor switches in the inverters are IGBTs Infineon FS50R12KE3. Dead time has been implemented in

hardware and is set to 6 μs. Dc voltage has been provided from an external dc source, Sorensen SGI 600/25, and was set to 600 V. An eleven-phase star-connected passive (*R-L*) load has been used, due to unavailability of the machine. It should be emphasised that using *R-L* load instead of a machine has no impact on any voltage-related considerations. The only difference is in the current analysis, which is beyond the scope of this paper. Value of the resistance (incandescent bulb) increases with increase of applied voltage and is therefore not constant, while the estimated value of the used inductance is 360 mH. Control algorithm is applied using $\sqrt{2}\cdot V/f = \text{const.}$ law with a knee of the characteristic at 300 V/50 Hz. Switching frequency has been set to 2 kHz. The photograph of the setup is shown in Fig. 7.

A block diagram of the utilised Simulink implementation of the SVPWM algorithm is shown in Fig. 8. It should be noted that for high phase numbers, such as 11, there are no commercially available DSPs with sufficient number of PWM outputs. Hence, an additional FPGA chip is typically used in such cases. Presented block diagram may be very useful for FPGA implementation especially if it can be directly programmed from the Simulink (as is possible for Xilinx FPGAs using Xilinx system generator).

It is obvious that switching sequences for all 22 sectors have to be stored in a memory. Also, calculation of duty cycles according to (9)-(10) slightly increases the computational burden of the algorithm. These are obviously main drawbacks compared to the carrier-based implementation. Note also that in the block for the final selection of the gating signals (bottom-right block in Fig. 8) a counter has to be used in order to keep each of the selected switching states for an appropriate amount of time (governed by duty cycles $\delta_0/4$, $\delta_1/2$, …) on the output. From this schematic it is clear why the carrier-based modulation is usually the preferred choice. However, shown space vector based implementation gives a better insight into the applied switching states and it provides additional flexibility that may be relevant for implementation of some specific modulation techniques (e.g. for non-symmetrical PWM).

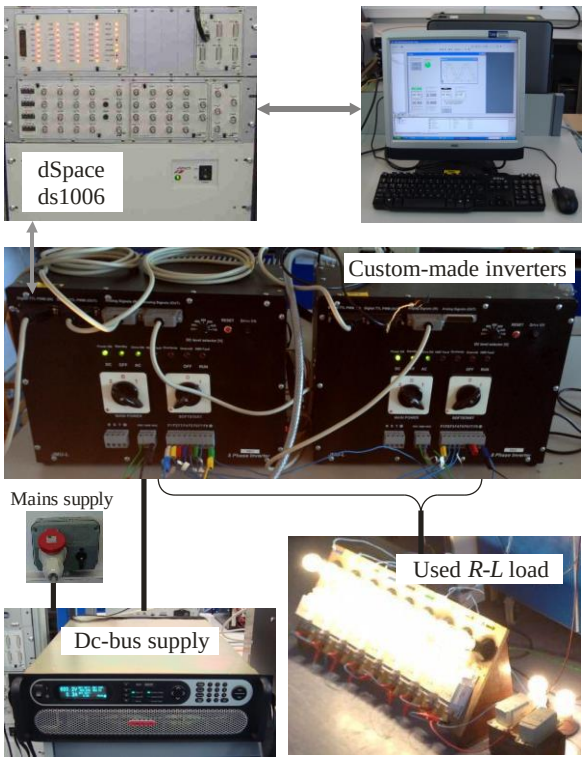

Fig. 7. Experimental setup.

Experiments are done for the whole linear modulation index range from 0.05 to 1 with a step of 0.05 and additionally for the maximum value in the linear range of 1.01, see (7). For each modulation index, leg voltage, phase voltage, and the phase current were measured. In addition, all the data have been processed later on, and spectra and THD of all measured variables have been calculated. Time-domain waveforms and spectra for the leg voltage, phase voltage and current, together with the phase voltage and current spectra, for $M = 0.5$ and $M = 1$ are shown in Fig. 9. Presence of a zero space vector (which leads to zero value in the phase voltage) in every switching period of the used space vector algorithm is obvious from the phase-voltage time-domain waveforms. From the voltage spectra one can see that the desired fundamentals (rms value of $M\cdot 300\text{V}/\sqrt{2}$) are almost achieved, with only slightly lower values caused by the dead-time effect. The step in the phase voltage is 600 V/11=54.54 V, as defined by (2), and the number of levels obtained in the phase voltage is 21 (as can be counted from Fig. 9b).

In order to compare behaviour of multiphase systems with different numbers of phases, the corresponding space vector algorithms have also been implemented for three-, five-, seven-, and nine-phase star-connected symmetrical *R-L* loads. The comparison is based on the phase voltage and current THD evaluation. THD is calculated, on the basis of the FFT, as:

$$\text{THD}_z = \sqrt{\sum_{k=2}^{h} Z_k^2} \Big/ Z_1 \qquad (13)$$

where z represents voltage or current, and Z_k stands for the k-th harmonic in the spectrum. Spectrum is calculated up to 21 kHz, which means that value of h is governed by the last harmonic in the spectrum whose frequency is lower than 21 kHz. Since the switching frequency is 2 kHz, this means that the first 10 side-bands are incorporated into the THD calculation in this way.

Obtained phase voltage and current THD curves in the modulation range from 0.2 up to the maximum modulation index value (with the step of 0.05) are shown in Fig. 10. It is interesting to notice that an increase in the number of phases will lead to an increase in the THD value under the same conditions. Indeed, Fig. 10 shows that the lowest phase voltage and current THDs are for the three-phase system. Also, one can see that for all the other numbers of phases (five, seven, nine and eleven) THD values are practically the same for the given modulation index. However, it should be noted that THD is a global figure of merit, and that this

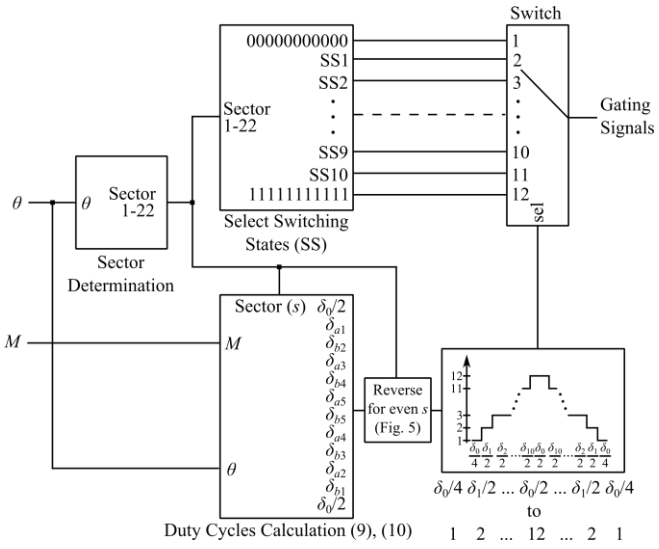

Fig. 8. Block diagram of the process used for implementation of the SVPWM algorithm.

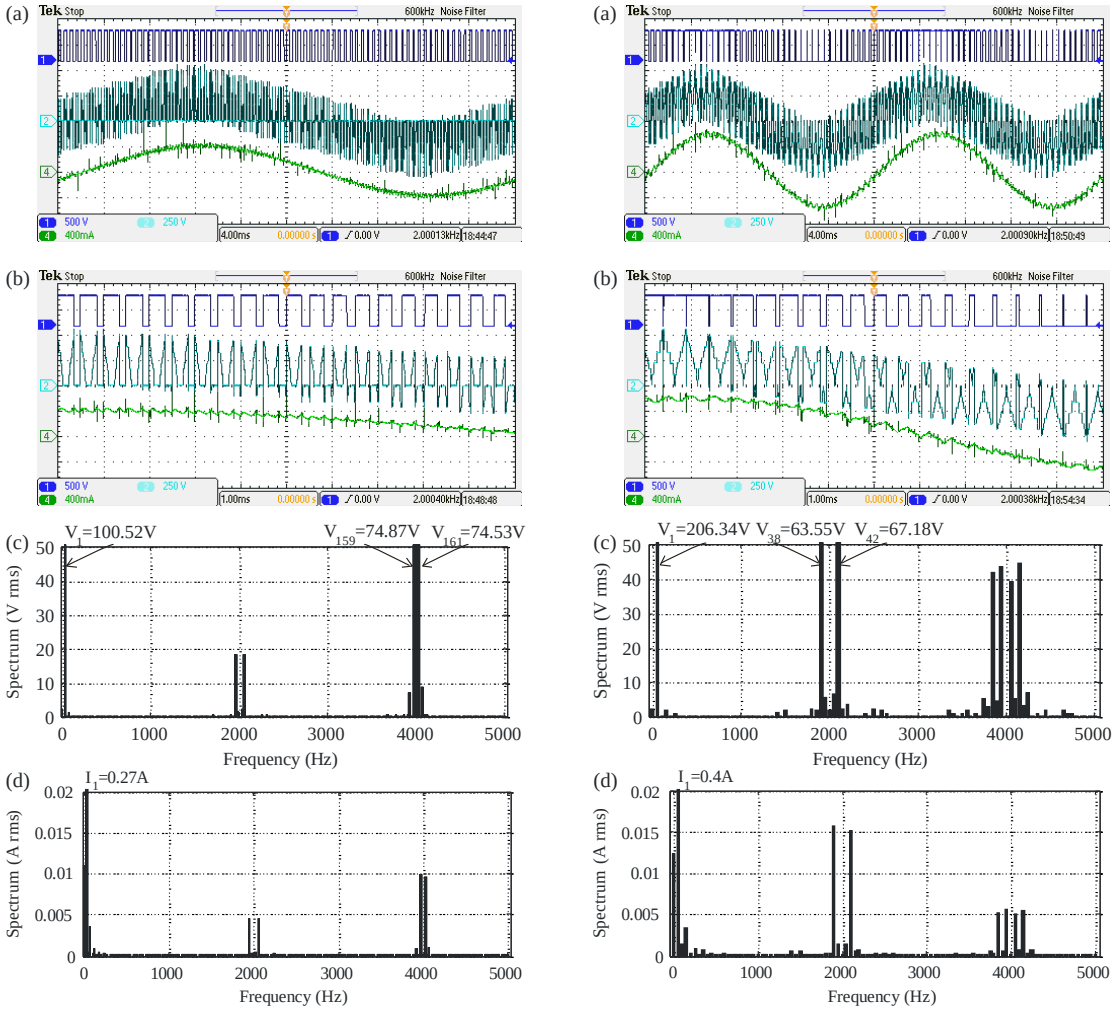

Fig. 9. (a) Oscilloscope recording of the leg and phase voltage, and load current for $M = 0.5$ (left) and $M = 1$ (right) (Ch1-leg voltage, 500 V/div; Ch2-phase voltage, 250 V/div; Ch4-phase current, 400 mA/div; time = 4 ms/div), and (b) with zoomed time scale (time = 1 ms/div), with associated (c) phase voltage and (d) current spectra.

result, which goes against increasing the number of phases above three, has to be put into a proper context that accounts for numerous advantages of the multiphase drive systems [1,2].

It is also worth noting that the trend exhibited by the voltage THD in Fig. 10a for the space vector PWM methods, used in conjunction with various multiphase systems, fully corresponds to the trend observed in [20] on the basis of derived purely analytical expressions for the sinusoidal carrier-based PWM techniques. Detailed analysis of the expression that represents the power of produced PWM phase voltage signal with a two-level inverter, derived in [20], shows that this can be represented as a function of the modulation index and the radius of the circle inscribed into the $2m$-sided polygon governed by the largest available vectors, i.e.

$$P = \frac{M}{\pi} r_{\max}(m) \tag{14}$$

Radius of the maximum circle $r_{\max}(m)$ that can be inscribed into the $2m$-sided polygon, governed by the largest set of vectors, increases with the increase in the phase number. On the other hand, the THD is proportional to the square root of the signal power (see [20]). Hence the value of THD for three-phase case is the smallest (Fig. 10a).

V. Conclusion

Space vector modulation for an 11-phase symmetrical load is investigated in this paper. Detailed explanations of the space vectors and their decomposition into five mutually decoupled planes are provided. As the desired output voltage is purely sinusoidal, the control is performed in the first (d-q) plane while simultaneous cancelation, on average per switching period, is obtained in all four auxiliary x-y planes through an appropriate space vector selection. Applied space vector algorithm is given in a general form, and, for the purpose of the comparison, it has been applied to the three-, five-, seven-, nine- and eleven-phase systems. Experimental results (time-domain waveforms and spectra) show proper functioning of the presented algorithm for the eleven-phase load. Comparison of the space vector PWM algorithm for different numbers of phases, by observing phase voltage and current THD, is also included. Obtained results show that while the three-phase system is characterised with the lowest values, all the other phase numbers are characterised with very similar, higher, values of the phase voltage and current THDs for a given modulation index value.

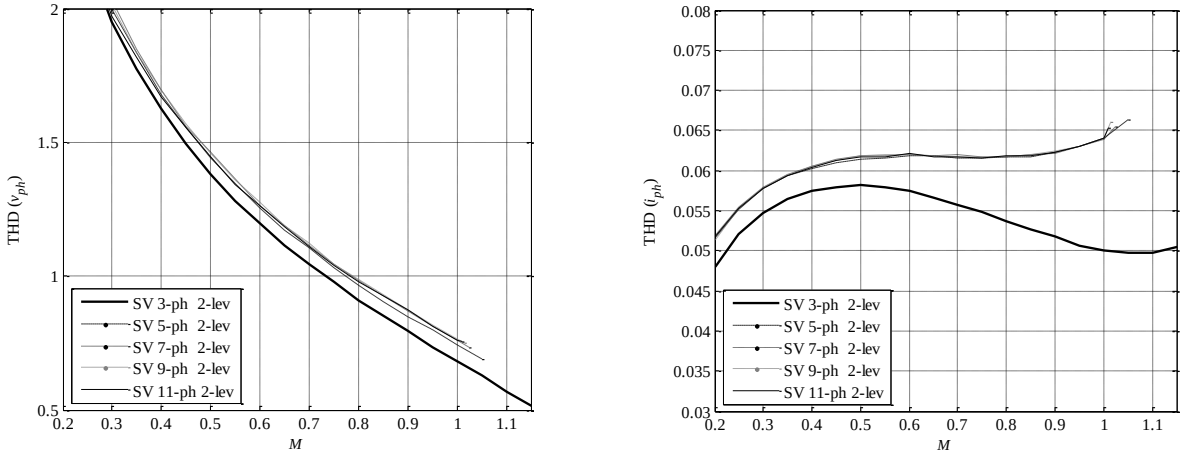

(a) (b)

Fig. 10. Phase voltage (a) and current (b) THDs, obtained experimentally, for three, five-, seven-, nine- and eleven-phase start-connected *R-L* load, for the linear modulation index range.

VI. Acknowledgment

This publication was made possible by the NPRP grant no. 04-152-02-53, from the Qatar National Research Fund (a member of The Qatar Foundation). The statements made herein are solely the responsibility of the authors.

VII. References

[1] E. Levi, R. Bojoi, F. Profumo, H.A. Toliyat, and S. Williamson, "Multiphase induction motor drives – A technology status review," *IET – Electric Power Applications*, vol. 1, no. 4, pp. 489-516, 2007.

[2] E. Levi, "Multiphase electric machines for variable-speed applications," *IEEE Trans. on Industrial Electronics*, vol. 55, no. 5, pp. 1893-1909, 2008.

[3] L. Gao and J.E. Fletcher, "A space vector switching strategy for three-level five-phase inverter drives," *IEEE Trans. on Industrial Electronics*, vol. 57, no. 7, pp. 2332-2343, 2010.

[4] O. Dordevic, E. Levi, and M. Jones, "A vector space decomposition based space vector PWM algorithm for a three-level seven-phase voltage source inverter", *IEEE Trans. on Power Electronics*, vol. 28, no. 2, pp. 637-649, 2013.

[5] G.D. Holmes and T.A. Lipo, "*Pulse width modulation for power converters – Principles and practice*", IEEE Press, John Wiley and Sons, Piscataway, NJ, USA, 2003.

[6] A. Iqbal, E. Levi,M. Jones, and S.N. Vukosavic, "Generalised, sinusoidal PWM with harmonic injection for multi-phase VSIs," *Proc.IEEE Power Electronics Spec. Conf. PESC,*Jeju, Korea, pp. 2871-2877, 2006.

[7] A. Iqbal, E. Levi, M. Jones, and S.N. Vukosavic, "A PWM scheme for a five-phase VSI supplying a five-phase two-motor drive," *Proc.IEEE Ind. Elec. Soc. Annual Meeting IECON*, Paris, France, pp. 2575-2580, 2006.

[8] J.W. Kelly, E.G. Strangas, and J.M. Miller, "Multi-phase space vector pulse width modulation", *IEEE Trans. on Energy Conversion*, vol. 18, no. 2, pp. 259-264, 2003.

[9] P.S. N. de Silva, J.E. Fletcher, and B.W. Williams, "Development of space vector modulation strategies for five-phase voltage source inverters", *Proc. IEE Power Electronics, Machines and Drives Conf., PEMD*, Edinburgh, UK, pp. 650-655, 2004.

[10] A. Iqbal and E. Levi, "Space vector PWM techniques for sinusoidal output voltage generation with a five-phase voltage source inverter", *Electric Power Components and Systems*, vol. 34, no. 2, pp. 119-140, 2006.

[11] G. Grandi, G. Serra, and A. Tani, "Space vector modulation of a seven-phase voltage source inverter," *Proc. Power Electronics, Electrical Drives, Automation and Motion Symp. SPEEDAM*, Taormina, Italy, pp. 1149-1156, 2006.

[12] G. Grandi, G. Serra, and A. Tani, "Space vector modulation of a nine-phase voltage source inverter", *Proc. IEEE International Symposium on Industrial Electronics ISIE*, Vigo, Spain, pp. 431-436, 2007.

[13] D. Dujic, G. Grandi, M. Jones, and E.Levi, "A space vector PWM scheme for multi-frequency output voltage generation with multi-phase voltage source inverters," *IEEE Trans. on Industrial Electronics*, vol. 55, no. 5, pp. 1943-195, 2008.

[14] D. Casadei, D. Dujić, E. Levi, G. Serra, A. Tani, and L. Zarri, "General modulation strategy for seven-phase inverters with independent control of multiple voltage space vectors," *IEEE Trans. on Industrial Electronics*, vol. 55, no. 5, pp. 1921-1932, 2008.

[15] A. Abdelkhalik, M. Masoud, and B. Williams, "Eleven-phase induction machine: steady-state analysis and performance evaluation with harmonic injection," *IET Electrical Power Applications*, vol. 4, no. 8, pp. 670–685, 2010.

[16] A.S. Abdel-Khalik, S.M. Gadoue, M.I. Masoud, and B.W. Williams, "Optimum flux distribution with harmonic injection for a multiphase induction machine using genetic algorithms," *IEEE Trans. on Energy Conversion*, vol. 26, no. 2, pp 501-512, 2011.

[17] A.S. Abdel-Khalik, M.I. Masoud, and B.W. Williams, "Improved flux pattern with third harmonic injection for multiphase induction machines," *IEEE Trans. on Power Electronics*, vol. 27, no. 3, pp. 1563-1578, 2012.

[18] S. Moinoddin, P. Rajeevan, H. Abu-Rub, and A. Iqbal, "Space vector modeling of an eleven-phase voltage source inverter," *Proc. IEEE Int. Conf. on Industrial Technology ICIT*, Cape Town, South Africa, pp. 1691 – 1696, 2013.

[19] D. Dujic, M. Jones, E. Levi, "Generalized space vector PWM for sinusoidal output voltage generation with multiphase voltage source inverters," *Int. J. Industrial Electronics and Drives*, vol. 1, no. 1, pp. 1-13, 2009.

[20] O. Dordevic, M. Jones, E. Levi, "Analytical formulas for phase voltage RMS Squared and THD in PWM multiphase systems," *IEEE Trans. on Power Electronics*, vol. 30, no. 3, pp. 1645-1656, 2015.